

Vortex precession frequency and its amplitude-dependent shift in cylindrical nanomagnets

Konstantin L. Metlov^{1, a)}

Donetsk Institute for Physics and Technology NAS, Donetsk, Ukraine 83114

(Dated: 2 November 2018)

Frequency of free magnetic vortex precession in circular soft ferromagnetic nano-cylinders (magnetic dots) of various sizes is an important parameter, used in design of spintronic devices (such as spin-torque microwave nano-oscillators) and characterization of magnetic nanostructures. Here, using a recently developed collective-variable approach to non-linear dynamics of magnetic textures in planar nano-magnets, this frequency and its amplitude-dependent shift are computed analytically and plotted for the full range of cylinder geometries. The frequency shift is positive in large planar dots, but becomes negative in smaller and more elongated ones. At certain dot dimensions a zero frequency shift is realized, which can be important for enhancing frequency stability of magnetic nano-oscillators.

PACS numbers: 75.78.Fg, 75.70.Kw, 75.75.Jn

Keywords: magnetization dynamics, magnetic nano-dots, magnetic vortex, anharmonism

Cylindrical magnetic nano-pillars with magnetic vortex are an important component of emerging spintronic applications, such as magnetic random access memory (MRAM)^{1,2} with ultra-fast core switching^{3,4} or spin-torque microwave nano-oscillators.⁵ The problem of non-linear magnetization dynamics in such systems poses a significant fundamental challenge. Only recently the amplitude-dependent frequency shift of vortex precession was probed experimentally in Ref. 6. This paper fully explores the problem of non-linear vortex precession in a circular magnetic nano-cylinder and describes the measured frequency shift⁶ quantitatively using a recently developed collective-variable approach to magnetization dynamics.⁷

Let us briefly remind the essentials of the approach. It is based on the Lagrangian formalism and allows to obtain the equations of motion for a magnetization texture, parametrized via a number of collective coordinates. A parametrization for a displaced magnetic vortex was developed earlier,⁸ which is a particular case of a more general family of trial functions⁹ and had already been successfully used in computing the vortex precession frequency in *large* planar magnetic dots.^{7,10} It is given by the following analytic function of complex variable

$$f(z) = \iota \frac{z - (A + \bar{A}z^2)}{r_V}, \quad (1)$$

where $\iota = \sqrt{-1}$, $z = X + \iota Y$; X , Y and Z are the Cartesian coordinates with the origin at the center of the cylinder (Z is parallel to its axis); $r_V = R_V/R$ is dimensionless vortex core radius and $A = A(t) = a_X(t) + \iota a_Y(t)$, $|A| < 1/2$ is a complex pair of collective coordinates. Position of the vortex center $f(z_C) = 0$ is $z_C = (1 - \sqrt{1 - 4A\bar{A}})/(2\bar{A})$. The centered vortex $z_C = 0$

corresponds to $A = 0$. An associated complex function⁹

$$w(z, \bar{z}) = \begin{cases} f(z) & |f(z)| \leq 1 \\ f(z)/\sqrt{f(z)\bar{f}(\bar{z})} & |f(z)| > 1 \end{cases}, \quad (2)$$

where the region $|f(z)| \leq 1$ corresponds to the vortex core (soliton) allows to recover the magnetization vectors $\vec{m} = \vec{M}/M_S$ via the stereographic projection $m_X + \iota m_Y = 2w/(1 + w\bar{w})$, $m_Z = \pm(1 - w\bar{w})/(1 + w\bar{w})$, which ensures that $|\vec{m}| = 1$. The \pm sign in m_Z corresponds to different polarizations of the vortex core: $m_Z = \pm 1$ at the vortex center. The function $w(z, \bar{z})$ is analytic inside the vortex core and non-analytic outside.

Dynamics of the magnetization texture (1) can be computed from its Lagrangian (normalized here by $\mu_0 M_S^2 \pi L_Z R^2$, where μ_0 is permeability of vacuum, L_Z is cylinder's thickness, R is its radius). Assuming the absence of the external driving forces and smallness of the vortex core center displacements $|A| \ll 1$, the Lagrangian has the form⁷

$$\mathcal{L} = \pm(\kappa_2 + \kappa_4(a_X^2 + a_Y^2))(a_X \dot{a}_Y - a_Y \dot{a}_X) - k_2(a_X^2 + a_Y^2) - k_4(a_X^2 + a_Y^2)^2 + \dots, \quad (3)$$

where the dot over variable denotes time derivative, $\kappa_2 = (1 + r_V^4(4 \log 2 - 3))/(\gamma \mu_0 M_S)$ and $\kappa_4 = 2 - r_V^2(23 + r_V^2((6061 - 6397r_V^2)/8 - 1152(1 - r_V^2) \log 2))/(\gamma \mu_0 M_S)$ have units of seconds, $\gamma \simeq 1.76 \cdot 10^{11}$ rad/(sT) is gyromagnetic ratio; k_2 and k_4 are dimensionless potential energy expansion coefficients. The first line in (3) is the kinetic energy and the second line is the negative potential energy of the vortex.

The equations of motion are the Euler-Lagrange equations extremizing the Lagrangian (3), they are

$$\begin{aligned} (\kappa_2 + 2\kappa_4(a_X^2 + a_Y^2))\dot{a}_X \pm (k_2 + 2k_4(a_X^2 + a_Y^2))a_Y &= \mathbf{0} \\ (\kappa_2 + 2\kappa_4(a_X^2 + a_Y^2))\dot{a}_Y \mp (k_2 + 2k_4(a_X^2 + a_Y^2))a_X &= \mathbf{0} \end{aligned} \quad (\mathbf{4})$$

For the initial conditions $a_X(0) = a_0$, $a_Y(0) = 0$ these equations are solved by⁷

$$a_X(t) = a_0 \cos(\omega t), \quad a_Y(t) = \pm a_0 \sin(\omega t) \quad (6)$$

^{a)} Electronic mail: metlov@fti.dn.ua

with

$$\omega = \frac{k_2 + 2a_0^2 k_4}{\kappa_2 + 2a_0^2 \kappa_4} \simeq \omega_0 + 2\alpha a_0^2 + \dots \quad (7)$$

$$\omega_0 = k_2/\kappa_2, \quad \alpha = \frac{k_4 \kappa_2 - k_2 \kappa_4}{\kappa_2^2}, \quad (8)$$

where α is the coefficient, relating the frequency of vortex rotation to its amplitude. These formulas are simple, but the dependence of the potential energy expansion coefficients k_2 and k_4 on cylinder dimensions can be rather complex. Evaluation and analysis of this dependence is the main subject of this work.

For the cylinder made of soft ferromagnetic material the main contributions to the potential energy come from the exchange and dipolar interactions. The exchange energy is simplest to evaluate, it is

$$E_{EX} = \frac{CM_S}{2} \iiint_V \sum_{i=X,Y,Z} (\vec{\nabla} m_i(\vec{r}))^2 d^3 \vec{r}, \quad (9)$$

where $C = 2A$ is the exchange stiffness and $\vec{\nabla} = \{\partial/\partial X, \partial/\partial Y, \partial/\partial Z\}$. For the magnetization distribution (1) the integration can be efficiently carried out using the residue theorem¹¹ even without assuming smallness of the vortex center displacements, which yields¹²

$$\begin{aligned} e_{EX} &= \frac{E_{EX}}{\mu_0 M_S^2 \pi L_Z R^2} = \frac{1}{\rho^2} \left(2 - \log \frac{2r_V}{1 + \sqrt{1 - 4|A|^2}} \right) \\ &= \frac{2 - \log r_V}{\rho^2} - \frac{|A|^2}{\rho^2} - \frac{3|A|^4}{2\rho^2} - \dots \end{aligned} \quad (10)$$

where $\rho = R/L_E$, $L_E = \sqrt{C/(\mu_0 M_S^2)}$ is the exchange length of cylinder's material. The exchange interaction is pushing the vortex out of the cylinder, as manifested by the negative signs before the powers of $|A|$.

Computation of the dipolar energy is more involved. To make it simpler, let us use the magnetostatic approximation by neglecting the time derivatives in Maxwell's equations and assuming that there are no macroscopic currents in the magnet. This approximation is justified *a posteriori* by noting that at characteristic GHz frequencies, obtained as the result of this computation, there is plenty of time for electromagnetic waves to propagate many times throughout the entire sub-micron ferromagnetic cylinder and, thus, for demagnetizing field to be velocity-independent. The magnetostatic approximation allows to introduce the *scalar* potential for demagnetizing field and express the magnetostatic energy as the interaction energy of magnetic charges with the density $-M_S(\vec{\nabla} \cdot \vec{m})$. Further, noting that at the boundary of the magnetic material the divergence is equal to the normal component of magnetization vector, magnetic charges can be subdivided into the surface charges (located at the faces of the cylinder in this case) and the volume charges (they become non-zero when vortex is displaced from the face center, $|A| > 0$). There are no surface charges on cylinder's side and also, due to symmetry (charges on the different faces have the opposite

sign), there is no interaction between the face and volume magnetic charges.

The energy of face charges (in the same normalization by $\mu_0 M_S^2 \pi L_Z R^2$) on both faces and their mutual interaction can be written as $e_f = U(0) - U(g)$ with

$$U(h) = \int_0^{2\pi} \int_0^{\theta(\varphi_1)} \int_0^{2\pi} \int_0^{\theta(\varphi_2)} u(h) d\varphi_1 dr_1 d\varphi_2 dr_2 \quad (11)$$

$$u(h) = \frac{m_Z(r_1, \varphi_1) m_Z(r_2, \varphi_2) r_1 r_2}{\sqrt{r_1^2 + r_2^2 - 2r_1 r_2 \cos(\varphi_1 - \varphi_2) + h^2}}, \quad (12)$$

where $g = L_Z/R$ is cylinder's aspect ratio and $r = \theta(\varphi)$ is the equation of vortex core boundary in polar coordinate system r, φ centered in the vortex center z_C , and with the origin of polar angle chosen to coincide with the direction of the complex phase of A . When $|A| = 0$ the vortex core boundary is a circle of radius r_V , for larger $|A|$ it becomes deformed. This deformation must necessarily be taken into account to obtain the correct values of magnetostatic energy. The equation for vortex core boundary is $f(r \exp(i\varphi) - z_C) = 1$. It has no explicit analytical solutions for r , but can be solved by $r = \theta(\varphi)$ in the form of Taylor series:

$$\frac{\theta(\varphi)}{r_V} = 1 + b_1 |A| + b_2 |A|^2 + b_3 |A|^3 + b_4 |A|^4 + \dots \quad (13)$$

with $b_1 = r_V \cos \varphi$, $b_2 = (5b_1^2 + 4 - r_V^2)/2$, $b_3 = b_1(8b_1^2 + 6 - 3r_V^2)$, $b_4 = (48 + 200b_1^4 + 231b_1^2 - 2(20 + 63b_1^2)r_V^2 + 7r_V^4)/8$. The density of the face charges is $m_Z(r, \varphi) = (r_V^2 - \beta^2)/(r_V^2 + \beta^2)$, with

$$\beta^2 = r^2(1 - |A|^2(4 - r^2)) - 2|A|r^3 \sqrt{1 - 4|A|^2} \cos \varphi \quad (14)$$

After the Taylor expansion m_Z also contains both even and odd powers of $|A|$ and also depends on φ . By carefully evaluating all the terms it is possible to obtain the following expansion for the magnetostatic energy of face charges

$$\begin{aligned} e_f &= \frac{r_V^3}{g} (W_{00}(\frac{g}{r_V}) + |A|^2 (W_{20}(\frac{g}{r_V}) + r_V^2 W_{22}(\frac{g}{r_V})) + \\ &|A|^4 (W_{40}(\frac{g}{r_V}) + r_V^2 W_{42}(\frac{g}{r_V}) + r_V^4 W_{44}(\frac{g}{r_V}))), \end{aligned} \quad (15)$$

where the magnetostatic functions W_i are defined in the Appendix A. The function $W_{00}(h)$ coincides with the magnetostatic function derived by Usov and Peschany¹³ for centered vortex.

The density of the volume charges is proportional to the negative divergence of the magnetization vector field $\Omega = -(\vec{\nabla} \cdot \vec{m})$, having different expressions inside and outside the vortex core

$$\Omega(r, \varphi) = \begin{cases} \frac{8|A|rr_V^3 \sin \varphi}{(r_V^2 + \beta^2)^2} & 0 \leq r < \theta(\varphi) \\ \frac{2|A|r \sin \varphi}{\beta} & \theta(\varphi) < r \leq \Theta(\varphi) \end{cases}, \quad (16)$$

where β is defined by (14) and $r = \Theta(\varphi)$ is the equation for cylinder boundary in the polar coordinate system,

centered in the vortex center z_C

$$\Theta(\varphi) = 1 - c_1|A| - c_2|A|^2 - c_3|A|^3 - c_4|A|^4 + \dots (17)$$

with $c_1 = \cos \varphi$, $c_2 = (1/2) \sin^2 \varphi$, $c_3 = \cos \varphi$, $c_4 = (17 - \cos(2\varphi) \sin^2 \varphi)/16$. The energy of the volume charges is then

$$e_v = \frac{1}{2g} \int_0^g dz_1 \int_0^{2\pi} d\varphi_1 \int_0^g dr_1 \int_0^{2\pi} d\varphi_2 \int_0^g dr_2 w \quad (18)$$

$$w = \frac{\Omega(r_1, \varphi_1) \Omega(r_2, \varphi_2) r_1 r_2}{\sqrt{r_1^2 + r_2^2 - 2r_1 r_2 \cos(\varphi_1 - \varphi_2) + (z_1 - z_2)^2}}, \quad (19)$$

where the factor 1/2 is due to the fact that each pair of interacting charges is summed twice during the double volume integration. Expanding it in powers of $|A|$ gives

$$e_v = |A|^2 V_2(r_V, g) + |A|^4 V_4(r_V, g) \quad (20)$$

with the magnetostatic functions V_i , defined in the Appendix B. While the volume magnetostatic functions are not much more complex, compared to the surface ones, they do not admit factorization of their dependence on r_V and g .

Collecting the terms in (10), (15), and (20) allows to recover the potential energy expansion coefficients

$$k_2 = -\frac{1}{\rho^2} + V_2 + \frac{r_V^3}{g} (W_{20} + r_V^2 W_{22}) \quad (21)$$

$$k_4 = -\frac{3}{2\rho^2} + V_4 + \frac{r_V^3}{g} (W_{40} + r_V^2 W_{42} + r_V^4 W_{44}), \quad (22)$$

where the arguments of the magnetostatic functions have been omitted for brevity and are the same as in (15), (20). Zero-order terms lead to the equation for the equilibrium vortex core radius^{11,13} $\rho_V = R_V/L_E$

$$-\frac{1}{\rho_V} + \frac{3\rho_V^2 W_{00}(\zeta/\rho_V)}{\zeta} - \rho_V W'_{00}(\zeta/\rho_V) = 0, \quad (23)$$

which depends only on cylinder's thickness $\zeta = L_Z/L_E$.

The formulae (21), (21), (23), and the definitions of magnetostatic functions contain all the ingredients necessary to compute the vortex precession frequency ω_0 and its shift α from (8). All these formulas are attached in the form of MATHEMATICA script `frequency.m` as a Supplemental Material.¹⁴ The computed frequencies and shifts are plotted in Figures 1 and 2 respectively. The selection of the coordinate system and range of parameters on these figures was done with intention to show the dependencies in full for as large set of dot geometries as possible. Consequently, some of the points in these figures may correspond to the dot dimensions beyond the applicability of the present model. At some of them the magnetic vortex might not be the ground state of the dot (see e.g. phase diagram in Ref. 15), or may be unstable^{12,16} at some of the larger included thicknesses the vortex might develop a 3-d structure, or its motion

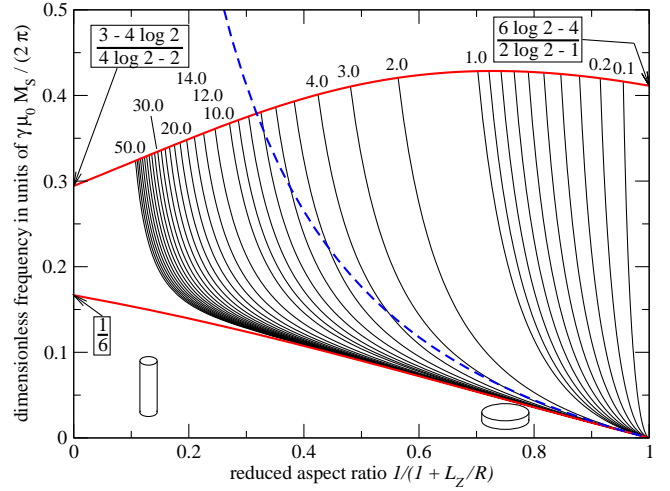


FIG. 1. Frequencies of free magnetic vortex precession in circular cylinder of radius R and thickness L_Z made of soft ferromagnetic material with saturation magnetization M_S and the exchange length L_E . The horizontal axis describes the cylinder's aspect ratio $g = L_Z/R$ with non-linear scale to cover all of its possible values. Thin solid lines correspond to different cylinder thicknesses, measured in units of L_E . The lines are sampled with several different equal steps in between the specified numerical labels. The lower bounding thick solid line shows the limit of large cylinders with negligible core, the upper thick solid line is for the cylinder radius exactly equal to the vortex core radius. The dashed line is the first order series expansion of the lower bounding line at $g = 0$. Formulas show the exact analytical expressions for frequencies at certain limiting geometries. Cylinder sketches illustrate shapes of cylinders at different ends of the horizontal axis.

will cause the spin-wave generation, making the high frequencies (on the left end of curves in Fig.1) unreachable. Also, plotting dependencies in full, has the drawback of blurring their fine details. To make plots with different scales and axes, please use the attached MATHEMATICA script `frequency.m` to compute the frequencies, shifts and potential energy expansion coefficients for an arbitrary cylinder geometry and material parameters.

There are several lessons, which can be learned from these graphs. First, the vortex precession frequency increases with decrease of the dot radius and increase of its thickness. The maximum is achieved when the particle radius coincides with the vortex core radius (the model is valid only when the vortex core fits completely inside the cylinder). It can be expected that due to overconfinement, resulting from the complete absence of the side charges, the vortex precession frequency for dots approaching the vortex core size is overestimated and can be considered an upper bound. Another computation, based on generalization of the trial function to relax the side boundary conditions^{9,17} may yield a better precision in the high-frequency region. For the low frequency region (corresponding to large dots) there is an established analytical approximation,^{7,10} based on neglecting the vortex core (assuming it is much smaller than the

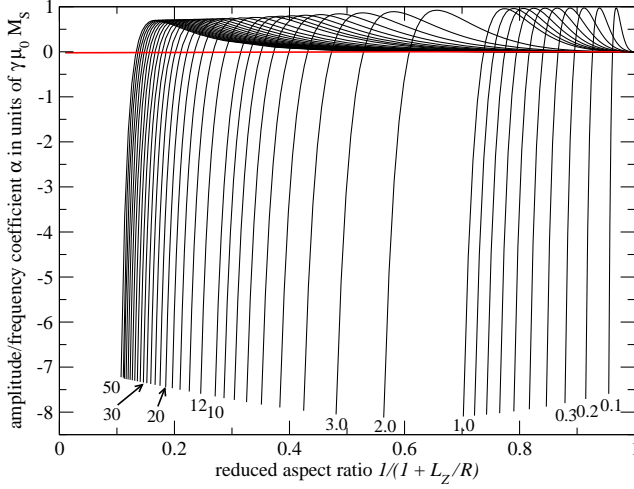


FIG. 2. Vortex precession frequency shift α at different cylinder geometries. The horizontal axis, parameters and thicknesses, corresponding to each of the line of the family, are the same as in Fig. 1.

particle size) $\omega_0 = \gamma\mu_0 M_S V_2(0, g)$ or

$$\nu_0 = \frac{\omega_0}{2\pi} = \frac{\gamma\mu_0 M_S}{\pi} \int_0^\infty \frac{f_{MS}(kg)}{k} \left[\int_0^1 r J_1(kr) dr \right]^2 dk, \quad (24)$$

$$\nu_0 \simeq \gamma\mu_0 M_S g \frac{2(2G - 1)}{6\pi^2}, \quad g \ll 1, \quad (25)$$

where $f_{MS}(x) = 1 - (1 - e^{-x})/x$ and $G \simeq 0.915966$ is Catalan's constant. The lower solid bounding line in Fig. 1 is exactly the Eq. 24. By noticing that it is very close to a straight line in the chosen coordinate system it is possible to obtain the following simple approximate analytical expression for the vortex precession frequency

$$\nu_0 \simeq \frac{\gamma\mu_0 M_S}{12\pi} \left(1 - \frac{1}{1+g} \right). \quad (26)$$

Unlike (25), shown in Fig. 1 by the dashed line, it does not contain the assumption of $g \ll 1$ and covers both flat and elongated cylinders. Compared to the full integral (24), it has the largest error of 7.91% at $g \approx 0.72$ or $1/(1 + 0.72) \approx 0.58$ decreasing for smaller and larger g .

The vortex frequency shift graph in Fig. 2 also covers the full range of cylinder geometries. Looking at (8) it can be *a priori* expected that the frequency shift may become negative. This is due to the negative term, proportional to κ_4 . This term describes the change of the vortex kinetic energy due to its shape deformation, which is missing in other computations, based on solution of Thiele equation.^{6,10,18-20} The Figure 2 confirms that it is indeed possible to have both positive (in cylinders with larger radii) and negative (in cylinders with smaller radii) frequency shifts. At a certain cylinder radius the frequency shift turns to zero. This feature can be useful for achieving high frequency stability of magnetic vortex precession. The shift is bounded from above by $\approx \gamma\mu_0 M_S$,

which is achievable in thin dots (about L_E in thickness). For thicker dots the maximum frequency shift is smaller.

The dimensionless frequency shift λ defined in Ref. 6 can be expressed as

$$\lambda = \frac{\alpha}{\omega_0} = \frac{k_4 \kappa_2 - k_2 \kappa_4}{k_2 \kappa_2}. \quad (27)$$

There is no additional factor despite the fact that α relates the frequency shift to $|A|^2$, while λ relates it to $|z_C|^2$. This is because to the first order the quantities A and z_C coincide, which is sufficient to obtain the same series expansion of (7). The experimental value of λ was determined for a single FeV dot in Ref. 6. Assuming the exchange length $6nm$ for their FeV crystal and the dot radius of $250nm$, which is the half of the minor axis of the studied elliptical dot that can be measured from the right half of the inset in their Fig.1, the Eq. 27 gives the relative frequency shift $\lambda = 0.38$, which is in agreement with the measured $\lambda = 0.5 \pm 30\%$.

Concluding, the series expansion of the magnetostatic energy of a cylindrical magnetic dot with a vortex is evaluated up to the fourth power in the vortex core center displacement, based on the model with no side magnetic charges (1). It allows to plot the vortex precession frequency (Fig. 1) and its amplitude-dependent shift (Fig. 2) for the full range of cylinder geometries. A simple algebraic expression for the vortex precession frequency (26) is proposed, which covers a wider set of cylinder geometries, compared to a similar relation^{7,10} (25). It is shown that the frequency shift can be positive and negative for certain dot geometries. For every cylinder thickness there is a cylinder radius for which the amplitude-dependent frequency shift is zero. The value of the shift is in agreement with the experimental data of Ref. 6.

Appendix A: Magnetostatic functions for face charges

When expanding the magnetostatic energy of face charges in powers of $|A|$ it is necessary to take into account that both integrand and integration limits depend on $|A|$ and to make proper use of the formula for taking the derivative of an integral, dependent on a parameter:

$$\frac{\partial}{\partial p} \int_{l_1(p)}^{l_2(p)} f(p, x) dx = \int_{l_1(p)}^{l_2(p)} \frac{\partial f(p, x)}{\partial p} dx + f(p, l_2(p)) l_2'(p) - f(p, l_1(p)) l_1'(p), \quad (A1)$$

where prime denotes the derivative. To factor the remaining angular and radial integrals, let us, as usual, represent the inverse square root via the Lipshitz integral

$$\frac{1}{\sqrt{b^2 + (z_1 - z_2)^2}} = \int_0^\infty e^{-k|z_1 - z_2|} J_0(kb) dk \quad (A2)$$

and use the Bessel's summation theorem for representing

$$J_0(k\sqrt{r_1^2 + r_2^2 - 2r_1 r_2 \cos(\varphi_1 - \varphi_2)}) =$$

$$\sum_{\mu=-\infty}^{\infty} J_{\mu}(kr_1)J_{\mu}(kr_2)e^{i\mu(\varphi_1-\varphi_2)}. \quad (\text{A3})$$

The magnetostatic energy of face charges is then expressed via the magnetostatic function

$$U(h) = \sum_{\mu=-\infty}^{\infty} \int_0^{\infty} e^{-kh} (i(\mu, k))^2 dk \quad (\text{A4})$$

$$i(\mu, k) = \int_0^{2\pi} d\varphi \int_0^{\theta(\varphi)} dr m_z(r, \varphi) r J_n(kr) e^{i\mu\varphi} \quad (\text{A5})$$

Expanding this expression in powers of $|A|$ and taking the angular integrals yields

$$e_f = \frac{r_V^3}{g} (W_{00}(g/r_V) + |A|^2 (W_{20}(g/r_V) + r_V^2 W_{22}(g/r_V)) + |A|^4 (W_{40}(g/r_V) + r_V^2 W_{42}(g/r_V) + r_V^4 W_{44}(g/r_V))) \quad (\text{A6})$$

with magnetostatic functions $W_i(h) = U_i(0) - U_i(h)$ and

$$i_0(k) = \int_0^1 \frac{1-r^2}{1+r^2} J_0(kr) r dr \quad (\text{A7})$$

$$U_{00}(h) = \int_0^{\infty} e^{-kh} (i_0(k))^2 dk \quad (\text{A8})$$

$$i_1(k) = \int_0^1 \frac{r^3}{(1+r^2)^2} J_0(kr) dr \quad (\text{A9})$$

$$U_{20}(h) = 16 \int_0^{\infty} e^{-kh} i_0(k) i_1(k) dk \quad (\text{A10})$$

$$i_2(k) = \frac{J_0(k)}{2} - 4 \int_0^1 \frac{r^5(1-r^2)}{(1+r^2)^3} J_0(kr) dr \quad (\text{A11})$$

$$i_3(k) = \int_0^1 \frac{r^4}{(1+r^2)^2} J_1(kr) dr \quad (\text{A12})$$

$$U_{22}(h) = \int_0^{\infty} e^{-kh} (i_0(k) i_2(k) + 8(i_3(k))^2) dk \quad (\text{A13})$$

$$i_4(k) = J_0(k) + 16 \int_0^1 \frac{r^5}{(1+r^2)^3} J_0(kr) r dr \quad (\text{A14})$$

$$U_{40}(h) = \int_0^{\infty} e^{-kh} (64(i_1(k))^2 + 4i_0(k) i_4(k)) dk \quad (\text{A15})$$

$$i_5(k) = -6J_0(k) + kJ_1(k) + 32 \int_0^1 \frac{r^7(2-r^2)}{(1+r^2)^4} J_0(kr) dr \quad (\text{A16})$$

$$i_6(k) = J_1(k) - 4 \int_0^1 \frac{r^4(1-3r^2)}{(1+r^2)^3} J_1(kr) dr \quad (\text{A17})$$

$$i_7(k) = 8i_2(k) i_1(k) - i_5(k) i_0(k) + 8i_3(k) i_6(k) \quad (\text{A18})$$

$$U_{42}(h) = \int_0^{\infty} e^{-kh} i_7(k) dk \quad (\text{A19})$$

$$i_8(k) = (62 - k^2) J_0(k) - 16kJ_1(k) + 128 \int_0^1 \frac{r^9(1-4r^2-r^4)}{(1+r^2)^5} J_0(kr) dr \quad (\text{A20})$$

$$i_9(k) = kJ_0(k) + 6J_1(k) - 32 \int_0^1 \frac{r^8(2-r^2)}{(1+r^2)^4} J_1(kr) dr \quad (\text{A21})$$

$$i_{10}(k) = \int_0^1 \frac{r^7}{(1+r^2)^3} J_2(kr) dr \quad (\text{A22})$$

$$i_{11}(k) = (J_2(k))^2 + 16i_3(k) i_9(k) + i_0(k) i_8(k) + 8(i_2(k))^2 + 32i_{10}(k) (J_2(k) + 8i_{10}(k)) \quad (\text{A23})$$

$$U_{44}(h) = \frac{1}{32} \int_0^{\infty} e^{-kh} i_{11}(k) dk \quad (\text{A24})$$

These expressions, while compact, are not easy to evaluate numerically, because of the k integration over infinite region of oscillating products of Bessel's functions. This difficulty is especially pronounced when evaluating $U_i(0)$, entering the magnetostatic functions $W_i(h)$. To alleviate this difficulty the actual numerical formulas in the MATHEMATICA file `frequency.m` are further rearranged by using the following identity III 6.612(3) in Ref. 21

$$\int_0^{\infty} e^{-kh} J_n(kr_1) J_n(kr_2) dk = \frac{Q_{n-1/2}((h^2 + r_1^2 + r_2^2)/(2r_1 r_2))}{\pi \sqrt{r_1 r_2}}, \quad (\text{A25})$$

where $Q_m(x)$ is the Legendre function of the second kind. Some of the remaining integrals were taken analytically. The result of this convergence improvement was checked against the original expressions above.

Appendix B: Magnetostatic functions for volume charges

The expansion of the energy of the volume charges in powers of $|A|$ can be factored using the Lipshitz integral and Bessel's summation theorem similarly to the energy of face charges. The integration across Z , can be carried out analytically

$$\frac{1}{2g} \int_0^g \int_0^g e^{-k|z_1-z_2|} dz_1 dz_2 = \frac{f_{\text{MS}}(kg)}{k} \quad (\text{B1})$$

$$f_{\text{MS}}(x) = 1 - \frac{1 - e^{-x}}{x}. \quad (\text{B2})$$

Taking the remaining angular and radial integrals produces

$$e_v = |A|^2 V_2(r_V, g) + |A|^4 V_4(r_V, g) \quad (\text{B3})$$

with the following magnetostatic functions

$$j_0(r_V, k) = 4r_V^3 \int_0^{r_V} \frac{r^2}{(r^2 + r_V^2)^2} J_1(kr) dr + \int_{r_V}^1 r J_1(k) dk \quad (\text{B4})$$

$$V_2(r_V, g) = 2 \int_0^{\infty} \frac{f_{\text{MG}}(kg)}{k} (j_0(r_V, k))^2 dk \quad (\text{B5})$$

$$j_1(r_V, k) = -J_2(k) + \int_{r_V}^1 r^2 J_2(kr) dr \quad (\text{B6})$$

$$j_2(r_V, k) = kJ_0(k) - 5J_1(k) + r_V^4 J_1(kr_V) +$$

$$\int_{r_V}^1 r(16 - r^2)J_1(kr) dr + 32r_V^3 \int_0^{r_V} \frac{r^4(r^4 + 8r_V^2 + 2r^2(4 - r_V^2))J_1(kr)}{(r^2 + r_V^2)^4} dr \quad (\text{B7})$$

$$j_3(r_V, k) = \int_0^{r_V} \frac{r^5 J_2(kr)}{(r^2 + r_V^2)^3} dr \quad (\text{B8})$$

$$j_4(r_V, k) = (j_1(r_V, k))^2 + j_0(r_V, k)j_2(r_V, k) + 32r_V^3 j_1(r_V, k)j_3(r_V, k) + 256r_V^6 (j_3(r_V, k))^2 \quad (\text{B9})$$

$$V_4(r_V, g) = \frac{1}{2} \int_0^\infty \frac{f_{\text{MG}}(kg)}{k} j_4(r_V, k) dk. \quad (\text{B10})$$

¹B. Van Waeyenberge, A. Puzic, H. Stoll, K. W. Chou, T. Tyliczszak, R. Hertel, M. Fähnle, H. Bruckl, K. Rott, G. Reiss, I. Neudecker, D. Weiss, C. H. Back, and G. Schutz, *Nature* **444**, 461 (2006).

²R. P. Cowburn, *Nature Mater.* **6**, 255 (Apr. 2007).

³K.-S. Lee, K. Y. Guslienko, J.-Y. Lee, and S.-K. Kim, *Phys. Rev. B* **76**, 174410 (2007).

⁴R. Hertel, S. Gliga, M. Fähnle, and C. M. Schneider, *Phys. Rev. Lett.* **98**, 117201 (2007).

⁵V. S. Pribyl, I. N. Krivorotov, G. D. Fuchs, P. M. Braganca, O. Ozatay, J. C. Sankey, D. C. Ralph, and R. A. Buhrman, *Nature Phys.* **3**, 498 (Jul. 2007).

⁶O. Sukhostavets, B. Pigeau, G. de Loubens, V. Naletov, O. Klein, K. Mitsuzuka, S. Andrieu, F. Montaigne, and K. Y. Guslienko, “Probing the anharmonicity of the potential well for magnetic vortex core in nanodot,” ArXiv:1307.5429.

⁷K. L. Metlov, *Phys. Rev. B* **88**, 014427 (2013).

⁸K. L. Metlov, “Two-dimensional topological solitons in soft ferromagnetic cylinders,” (2001), arXiv:cond-mat/0102311.

⁹K. L. Metlov, *Phys. Rev. Lett.* **105**, 107201 (2010).

¹⁰K. Y. Guslienko, X. F. Han, D. J. Keavney, R. Divan, and S. D. Bader, *Phys. Rev. Lett.* **96**, 067205 (2006).

¹¹K. L. Metlov, *J. Magn. Magn. Mater.* **343**, 55 (2013).

¹²K. L. Metlov and K. Y. Guslienko, *J. Magn. Magn. Mater.* **242–245**, 1015 (2002).

¹³N. A. Usov and S. E. Peschany, *J. Magn. Magn. Mater.* **118**, L290 (1993).

¹⁴See supplementary material as [URL will be inserted by AIP] for Mathematica code computing potential energy expansion coefficients and vortex precession frequency.

¹⁵K. L. Metlov and Y. P. Lee, *Appl. Phys. Lett.* **92**, 112506 (2008).

¹⁶N. A. Usov and S. E. Peschany, *Fiz. Met. Metal* (in Russian) **12**, 13 (1994).

¹⁷K. L. Metlov and K. Y. Guslienko, *Phys. Rev. B* **70**, 052406 (2004).

¹⁸B. A. Ivanov and C. E. Zaspel, *Phys. Rev. Lett.* **99**, 247208 (Dec. 2007).

¹⁹K. Y. Guslienko, R. H. Heredero, and O. Chubykalo-Fesenko, *Phys. Rev. B* **82**, 014402 (Jul 2010).

²⁰A. Dussaux, A. V. Khvalkovskiy, P. Bortolotti, J. Grollier, V. Cros, and A. Fert, *Phys. Rev. B* **86**, 014402 (Jul 2012).

²¹I. S. Gradshteyn and I. M. Ryzhik, *Tables of series, products, and integrals* (Gos. izdatelstvo fiz.-mat. literatury, Moskva, 1963).